Two-Image Perspective Photometric Stereo Using Shape-from-Shading

Roberto Mecca[1], Ariel Tankus[2], and Alfred Marcel Bruckstein[1]

[1] Department of Computer Science, Technion - Israel Institute of Technology
[2] Department of Biomedical Engineering, Technion - Israel Institute of Technology

Abstract. Shape-from-Shading and photometric stereo are two fundamental problems in Computer Vision aimed at reconstructing surface depth given either a single image taken under a known light source or multiple images taken under different illuminations, respectively. Whereas the former utilizes partial differential equation (PDE) techniques to solve the image irradiance equation, the latter can be expressed as a linear system of equations in surface derivatives when 3 or more images are given. It therefore seems that current photometric stereo techniques do not extract all possible depth information from each image by itself. This paper utilizes PDE techniques for the solution of the combined Shape-from-Shading and photometric stereo problem when only 2 images are available. Extending our previous results on this problem, we consider the more realistic perspective projection of surfaces during the photographic process. Under these assumptions, there is a unique weak (Lipschitz continuous) solution to the problem at hand, solving the well known convex/concave ambiguity of the Shape-from-Shading problem. We propose two approximation schemes for the numerical solution of this problem, an up-wind finite difference scheme and a Semi-Lagrangian scheme, and analyze their properties. We show that both schemes converge linearly and accurately reconstruct the original surfaces. In comparison with a similar method for the orthographic 2-image photometric stereo, the proposed perspective one outperforms the orthographic one. We also demonstrate the method on real-life images. Our results thus show that using methodologies common in the field of Shape-from-Shading it is possible to recover more depth information for the photometric stereo problem under the more realistic perspective projection assumption.

1 Introduction

Reconstruction of three dimensional surface shape is one of the most fundamental problems in Computer Vision. Two reconstruction approaches, both of which first introduced in the 1970s, are Shape-from-Shading (SfS) [1] and photometric stereo [2,3]. Shape-from-Shading is aimed at solving the image irradiance equation, which relates the reflectance map to image intensity. Photometric stereo is a monocular 3D shape reconstruction method based on several images of a scene taken from an identical viewpoint under different illumination conditions. The most common approach in the field divides the task into two: recovery of surface

K.M. Lee et al. (Eds.): ACCV 2012, Part IV, LNCS 7727, pp. 110–121, 2013.

gradients and integration of the resultant gradient field to determine the 3D surface itself. The goal of the first part is to solve a system of image irradiance equations. When given 3 or more images, this system becomes linear. As such, the gradient field can be recovered analytically. For this reason, Shape-from-Shading and photometric stereo have very diverse methodologies, even though the latter is a generalization of the former.

A more recent development in the field of Shape-from-Shading is the transition from the assumption of an orthographic projection of the photographed surface onto the image plane to an assumption of perspective projection [4,5,6,7,8,9,10]. Perspective Shape-from-Shading algorithms were shown to outperform state-of-the-art orthographic techniques ([4]) and be applicable to real-life images ([7]).

Photometric stereo research has focused on reconstruction from three or more images (see [11] for a review). Conditions on the illumination and surface reflectance required to obtain uniqueness of solution for three light source photometric stereo are described by Okatani and Deguchi [12]. Even when the light source intensity and directions are unknown, Shashua [13] has shown that three or more images provide enough information to determine the scaled surface normals of an object up to an unknown linear transformation, which allows the reconstruction of the surface also under unknown lighting conditions (assuming distant light sources) [14].

For this reason, only few studies investigated the problem of 2-image photometric stereo (for example, [15,16,17]). A comprehensive work on existence and uniqueness in 2-image photometric stereo is that of Kozera [18]. Mecca and Falcone [16] extended some of the results of Kozera [18] and Onn and Bruckstein [15], proving a uniqueness result for weak (Lipschitz continuous) solutions. They also proposed two approximation schemes for the numerical solution of this problem: an up-wind finite difference scheme and a Semi-Lagrangian scheme.

Tankus and Kiryati [19] changed the common orthographic projection assumption in photometric stereo to a perspective one (similar to Tankus et al. [4] in Shape-from-Shading), and found an analytic linear solution for the gradient field of a 3-image perspective photometric stereo problem. Yoon et al. [20] employed a variational framework in their perspective photometric stereo algorithm, and demonstrated it using a large sets of input images (≥ 16).

Whereas 2-image orthographic photometric stereo has been investigated for extracting more information from each equation using Shape-from-Shading techniques, and 3-image perspective photometric stereo has an analytical solution for the gradient field, no information is available on the 2-image photometric stereo problem under the perspective projection model. The goal of this research is thus to utilize numerical schemes commonly used in the Shape-from-Shading realm also for 2-image photometric stereo under the perspective projection assumption, thus extracting additional information from each given image. We prove a uniqueness result for weak (Lipschitz continuous) solutions under the perspective projection model, and propose two numerical approxiamtion schemes: an up-wind finite difference scheme and a Semi-Lagrangian scheme. This paper

thus extends and combines three research directions, by Mecca and Falcone [16], Tankus and Kiryati [19], and Onn and Bruckstein [15].

The paper is organized as follows. Following the description of notations and assumptions (Sect. 2), we formulate the new differential model for the photometric stereo problem (Sect. 3) and we then prove the uniqueness of weak solution for the new differential model (Sect. 4). In Section 5 we suggest approximation schemes for the perspective photometric stereo-Shape-from-Shading problem. We demonstrate the performance of the suggested schemes by a comparison with the orthographic schemes [16] (Section 6). Concluding remarks appear in Section 7.

2 Notations and Assumptions

Let us fix the main ingredients for the formulation of the model for the Perspective Shape from Shading (PSfS) presented in [21]:

- the light source is given by a unit vector $\omega = (\omega_1, \omega_2, \omega_3)$ (with $\omega_3 < 0$);
- the surface in the real world is given by the analytical function $h(x, y) = (x, y, \hat{z}(x, y))$ (where the point (x, y) is in the image domain $\overline{\Omega} = \Omega \cup \partial\Omega$, on the optical plane);
- the associated perspective surface is given by the function $k(\xi, \eta) = (\xi, \eta, z(\xi, \eta))$ (where the point (ξ, η) is in the perspective image domain $\overline{\Omega^p} = \Omega^p \cup \partial\Omega^p$, on the focal plane, parallel to the optical one at a focal distance f);
- the transformation used to pass from one point in the optical plane (x, y) to the respective one in the focal plane is $\xi = -\frac{x}{\hat{z}(x,y)} f$, $\eta = -\frac{y}{\hat{z}(x,y)} f$. Then we have: $k(\xi, \eta) = (\xi, \eta, z(\xi, \eta)) = \big(-\frac{x}{\hat{z}(x,y)} f, -\frac{y}{\hat{z}(x,y)} f, \hat{z}(x, y)\big)$.

3 The New Photometric Stereo Differential Model

Now, considering the irradiance equation given by the inner product between the light source ω and the normal vector to the surface $k(\xi, \eta)$ [21], we have the following differential problem (non-linear PDE + Dirichlet boundary condition):

$$\begin{cases} \rho(\xi,\eta)\dfrac{-z_\xi(f\omega_1 + \xi\omega_3) - z_\eta(f\omega_2 + \eta\omega_3) - z\omega_3}{\sqrt{f^2(z_\xi^2 + z_\eta^2) + (z + \xi z_\xi + \eta z_\eta)^2}} = I(\xi,\eta), \text{ on } \Omega^p; \\ z(\xi,\eta) = g(\xi,\eta) \qquad\qquad\qquad\qquad\qquad\qquad \text{on } \partial\Omega^p; \end{cases} \tag{1}$$

which has no unique solution even if the albedo $\rho(\xi, \eta)$ is known.

Let us try to overpass the problem of uniqueness of solution considering the Photometric Stereo (PS) approach using two light sources defined by the unit vectors $\omega' = (\omega'_1, \omega'_2, \omega'_3)$ and $\omega'' = (\omega''_1, \omega''_2, \omega''_3)$ (with ω'_3, $\omega''_3 < 0$).

Using the information obtained by both images we can couple the two equations related to the irradiance equation in (1) obtaining the following system of non-linear PDE:

$$\begin{cases} \rho(\xi,\eta)\dfrac{-z_\xi(f\omega_1'+\xi\omega_3')-z_\eta(f\omega_2'+\eta\omega_3')-z\omega_3'}{\sqrt{f^2(z_\xi^2+z_\eta^2)+(z+\xi z_\xi+\eta z_\eta)^2}} = I_1(\xi,\eta), & \text{on } \Omega^p; \\ \rho(\xi,\eta)\dfrac{-z_\xi(f\omega_1''+\xi\omega_3'')-z_\eta(f\omega_2''+\eta\omega_3'')-z\omega_3''}{\sqrt{f^2(z_\xi^2+z_\eta^2)+(z+\xi z_\xi+\eta z_\eta)^2}} = I_2(\xi,\eta), & \text{on } \Omega^p; \\ z(\xi,\eta) = g(\xi,\eta) & \text{on } \partial\Omega^p. \end{cases} \tag{2}$$

Now, observing that the denominator of both equations is the same (i.e. it does not depend on the light source) and obviously always different from zero, we can explicit the non-linearity from the first equation for example

$$\sqrt{f^2(z_\xi^2+z_\eta^2)+(z+\xi z_\xi+\eta z_\eta)^2} = \frac{-z_\xi(f\omega_1'+\xi\omega_3')-z_\eta(f\omega_2'+\eta\omega_3')-z\omega_3'}{I_1(\xi,\eta)}\rho(\xi,\eta) \tag{3}$$

and replacing it in the other, we obtain the following linear problem

$$\begin{cases} b(\xi,\eta)\nabla z(\xi,\eta)+s(\xi,\eta)z(\xi,\eta)=0, & \text{on } \Omega^p; \\ z(\xi,\eta)=g(\xi,\eta) & \text{on } \partial\Omega^p. \end{cases} \tag{4}$$

Where:

$$\begin{aligned} b(\xi,\eta) = ((f\omega_1'+\xi\omega_3')I_2(\xi,\eta)-(f\omega_1''+\xi\omega_3'')I_1(\xi,\eta), \\ (f\omega_2'+\eta\omega_3')I_2(\xi,\eta)-(f\omega_2''+\eta\omega_3'')I_1(\xi,\eta)) \end{aligned} \tag{5}$$

and

$$s(\xi,\eta) = \omega_3' I_2(\xi,\eta) - \omega_3'' I_1(\xi,\eta). \tag{6}$$

It is clear that the albedo function disappears during the substitution of (3). This means that our new formulation of the PSfS-PS does not depend on the albedo, rather it is possible to compute it a posteriori.

4 Uniqueness of Weak Solution for the New Differential Model

With the aim to prove the uniqueness of weak (Lipschitz) solution of the differential problem (4) we start with the following:

Lemma 1. *If there are not any points $(\xi,\eta) \in \overline{\Omega}^p$ of black shadows for the image functions (i.e. $I_1(\xi,\eta) \neq 0$ and $I_2(\xi,\eta) \neq 0$), we have that $|b(\xi,\eta)| \neq 0$ (i.e. the vectorial function does not vanish in $\overline{\Omega}^p$).*

If we consider as a solution surface $\hat{z}(x,y)$ a Lipschitz one, and we consider the points where it is not differentiable as the family of regular curves $(\gamma_1(t),\ldots,\gamma_k(t))$ where t is the argument of the parametric representation, it is clear that this curve contains also the points of discontinuity of the image functions $I_1(\xi,\eta)$ and $I_2(\xi,\eta)$. Now, since the functions $b(\xi,\eta)$ and $s(\xi,\eta)$ depend directly on $I_1(\xi,\eta)$ and $I_2(\xi,\eta)$, the same family of curve represents the

discontinuity also for these coefficients of the PDE in (4). That is, if we consider our differential problem like an inverse problem of PSfS with photometric stereo technique, searching for a weak solution implies a study of the linear partial differential equation with discontinuous coefficients. Moreover there is a relation between the set of points of discontinuity of $b(\xi,\eta)$ and $s(\xi,\eta)$ and the set of points where the solution $\hat{z}(x,y)$ is not differentiable. In fact they are linked with a bijective correspondence due to the perspective. Another feature about the discontinuity type of $b(\xi,\eta)$ and $s(\xi,\eta)$ is always related to the fact that we are considering an inverse problem where it is proposed to find a Lipschitz solution. This means that it must be a jump discontinuity.

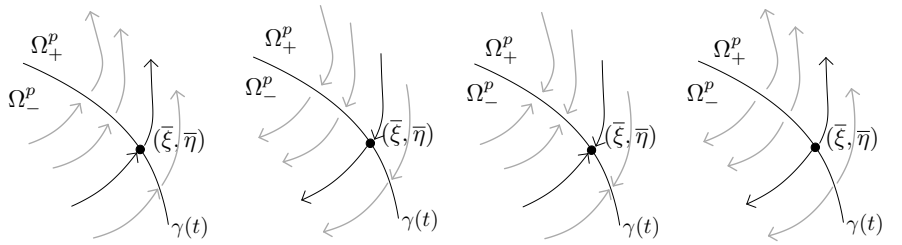

Fig. 1. All the possibles behaviors of the characteristic field close to the discontinuity curve $\gamma(t)$. The only admissible cases (that permits to the information to travel along the characteristic curves) are the first two from the left.

Theorem 2. *Let $\gamma(t)$ be a curve of discontinuity for the function $b(\xi,\eta)$ (and $f(\xi,\eta)$) and let $\overline{p} = (\overline{\xi},\overline{\eta})$ be a point of this curve. Let $n(\overline{\xi},\overline{\eta})$ be the outgoing normal with respect to the set Ω^p_+, than we have*

$$\left[\lim_{\substack{(\xi,\eta)\to(\overline{\xi},\overline{\eta})\\(\xi,\eta)\in\Omega^p_+}} b(\xi,\eta)\cdot n(\overline{\xi},\overline{\eta})\right]\left[\lim_{\substack{(\xi,\eta)\to(\overline{\xi},\overline{\eta})\\(\xi,\eta)\in\Omega^p_-}} b(\xi,\eta)\cdot n(\overline{\xi},\overline{\eta})\right] \geq 0 \tag{7}$$

A schematic explanation of the behavior of the vector field b described by this last theorem is represented in Fig. 1.

Theorem 3. *Let us consider the problem*

$$\begin{cases} b(\xi,\eta)\cdot\nabla z(\xi,\eta) + s(\xi,\eta)z(\xi,\eta) = 0, \text{ a.e. } (\xi,\eta)\in\Omega^p; \\ z(\xi,\eta) = g(\xi,\eta) \qquad\qquad\qquad\qquad \forall(\xi,\eta)\in\partial\Omega^p. \end{cases} \tag{8}$$

Let us suppose that $(\gamma_1(t),\ldots,\gamma_k(t))$, the family of discontinuity curves for $b(\xi,\eta)$ and $s(\xi,\eta)$, are not characteristic curves (with respect to the previous problem). Then there exists a unique Lipschitz solution of the problem.

A sketch of the proof of the previous and main theorem can easily obtained looking at Lemma 1 and Theorem 2. They can be considered as the main ingredients which permit to make travel the information stored on the boundary condition $g(\xi,\eta)$ across all the domain Ω^p. The trajectories followed are defined by the vector field $b(\xi,\eta)$ which has all the good properties to make Theorem 8 proved.

5 Some Approximation Schemes for the Perspective SfS-PS Linear Equation

For the numerical schemes we consider the domain $\overline{\Omega}^p = [a^p, b^p] \times [c^p, d^p]$. The discretization space steps are $\Delta_\xi = (b^p - a^p)/n$ and $\Delta_\eta = (c^p - d^p)/m$ where n and m are the number of intervals divide the sides of the rectangular domain (that is $\xi_i = a^p + i\Delta_\xi$, $\eta_j = c^p + j\Delta_\eta$ with $i = 0, \ldots, n$ and $j = 0, \ldots, m$). We will denote by $\overline{\Omega}^p_d$ all the points of the lattice belonging to $\overline{\Omega}^p$, by Ω^p_d all the internal points and by $\partial\Omega^p_d$ all the boundary points.

5.1 Finite Difference

Forward Up-Wind Scheme. In order to introduce a finite difference numerical scheme which does not need to consider a particular direction of the vector field b in order to be well defined, let us consider the following implicit up-wind scheme:

$$b^1_{i,j}\frac{Z^F_{i+1,j} - Z^F_{i-1,j}}{2\Delta_\xi} + b^2_{i,j}\frac{Z^F_{i,j+1} - Z^F_{i,j-1}}{2\Delta_\eta} + s_{i,j}Z^F_{i,j} = |b^1_{i,j}|\frac{Z^F_{i+1,j} - 2Z^F_{i,j} + Z^F_{i-1,j}}{2\Delta_\xi} + |b^2_{i,j}|\frac{Z^F_{i,j+1} - 2Z^F_{i,j} + Z^F_{i,j-1}}{2\Delta_\eta} \quad (9)$$

for $i = 1, \ldots, n-1$ and $j = 1, \ldots, m-1$. The artificial diffusion introduced in the right side of (9) allows to follow the vector field b considering the most appropriate discretization for the fist derivative in order to follow the characteristic lines ([22,23]).

The computation of Z^F consists of solve a global linear system where all the internal point of the grid are included. This means that the dimension of the system is $[(n-1)(m-1)] \times [(n-1)(m-1)]$. In order make understandable how we compute the matrix, we rewrite the (9) as follow:

$$Z^F_{i+1,j}\left(\frac{b^1_{i,j} - |b^1_{i,j}|}{2\Delta_\xi}\right) - Z^F_{i-1,j}\left(\frac{b^1_{i,j} + |b^1_{i,j}|}{2\Delta_\xi}\right) + Z^F_{i,j}\left(\frac{|b^1_{i,j}|}{\Delta_\xi} + \frac{|b^2_{i,j}|}{\Delta_\eta} + s_{i,j}\right) + Z^F_{i,j+1}\left(\frac{b^2_{i,j} - |b^2_{i,j}|}{2\Delta_\eta}\right) - Z^F_{i,j-1}\left(\frac{b^2_{i,j} + |b^2_{i,j}|}{2\Delta_\eta}\right) = 0. \quad (10)$$

This numerical scheme works forward with respect to the characteristics direction. This means that the information propagates starting from the inflow side of the boundary. In the numerical test are presented also results about the backward up-wind scheme.

5.2 Semi-lagrangian Discretization

A second numerical approach that permits to the solve equation (8) miming the propagation of the information along the characteristics is the following

semi-Lagrangian scheme. We pass then to consider the following equivalent equation obtained dividing the two sides of (8) by the norm of $b(\xi,\eta)$:

$$\nabla_\alpha z(\xi,\eta) + \frac{s(\xi,\eta)}{|b(\xi,\eta)|} z(\xi,\eta) = 0, \quad \forall (\xi,\eta) \in \Omega^p \tag{11}$$

with $\alpha(\xi,\eta) = \frac{b(\xi,\eta)}{|b(\xi,\eta)|}$.

We observe that the division by $|b(\xi,\eta)|$ doesn't involve any kind of difficulties for the numerical scheme (Lemma 1). Now, considering the definition of directional derivative, we can write:

$$\frac{z(\xi + h\alpha_1(\xi,\eta), \eta + h\alpha_2(\xi,\eta)) - z(\xi,\eta)}{h} + \frac{s(\xi,\eta)}{|b(\xi,\eta)|} z(\xi,\eta) \simeq 0, \quad \forall (\xi,\eta) \in \Omega^p \tag{12}$$

Considering a uniform discretization $\overline{\Omega}^p_d$ as in the previous section, we can finally write the semi-Lagrangian schemes:

$$z^{n+1}_{i,j} = z^n(\xi_i + h\alpha_1(\xi_i,\eta_j), \eta_j + h\alpha_2(\xi_i,\eta_j)) \frac{|b_{i,j}|}{|b_{i,j}| - hs_{i,j}} \quad \forall (\xi_i,\eta_j) \in \Omega^p_d \tag{13}$$

where $z^n(\xi_i,\eta_j) = z^n_{i,j}$ and $z^{n+1}(\xi_i,\eta_j) = z^{n+1}_{i,j}$ defined only on the grid nodes. In order to include the boundary condition on the scheme we assign an initial function $z^0_{i,j}$, such that $z^0(\xi_i,\eta_j) = g(\xi_i,\eta_j)\ \forall (\xi_i,\eta_j) \in \partial\Omega^p_d$.

This numerical scheme works backward with respect to the direction of the characteristics. This means that it will need of the boundary data on the outflow part of $\partial\Omega$. Also for this semi-Lagrangian scheme the forward version has been developed and the results are presented in the next section.

6 Numerical Tests

This section describes the experiments conducted with the proposed numerical schemes: the Semi-Lagrangian and the up-wind finite difference scheme, each in its forward and backward formulation.

For the numerical tests we utilized three surfaces (see Fig. 2), each with a different geometrical and analytical characteristics.

For each of these surfaces, we computed its perspective image under two light source directions according to the procedure described by Tankus et al. [4] (Fig. 3). We used a constant focal length $f = 1$ for all images. In all numerical tests, the albedo was set to $\rho = 1$ in all image domains except for the dark stripe in each of the images (see Fig. 3), where it was set to $\rho = 0.5$. We repeated the experiements with images of several sizes: 100×100, 200×200, 400×400, and 800×800 pixels.

Reconstruction by the suggested perspective Semi-Lagrangian and up-wind schemes is highly accurate, as demonstrated in Fig. 5.

We compared the suggested numerical methods for solving the perspective photometric stereo problem with the ones suggested by Mecca and Falcone [16]

for solving the equivalent orthographic photometric stereo problem. Whereas the orthographic methods converge and yield an accurate reconstruction of the aforementioned surfaces when images were generated by orthographic projection [16], the accuracy is compromised when required to reconstruct images generated by a more realistic photographic process: perspective projection (Fig. 4). The suggested perspective methods, on the other hand, faithfully reconstructed all surfaces, despite the irregularities (Fig. 5).

Three error measures comparing the reconstructed and true surfaces are provided for each scheme: the L^∞ norm in the perspective coordinate system $(\xi, \eta, z(\xi, \eta))$, root mean square error (RMSE) in the perspective coordinate system $(\xi, \eta, z(\xi, \eta))$, and RMSE in real-world coordinate system $(x, y, \hat{z}(x, y))$ (perspective: tables 1 and 2; orthographic: table 3). The L^∞ norm allows us to examine the convergence rate of the numerical schemes, showing that both perspective schemes converges linearly (i.e., with order 1), because doubling the number of grid nodes halves the error. The orthographic method did not converge on the surfaces examined. The RMSE measure, on the other hand, has the same units as surface depth, and therefore quantifies the mean error with respect to the original surface. This measure can be easily compared to the aforementioned ranges of $\hat{z}(x, y)$ values. The RMSE of the perspective reconstruction is an order of magnitude smaller than that of the orthographic reconstruction (cf. Tables 1 and 2 with Table 3).

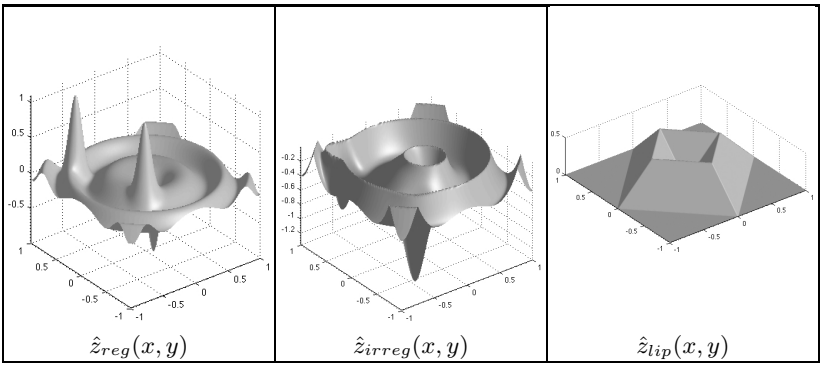

Fig. 2. Set of surfaces used for the numerical tests, each with different geometrical and analytical characteristics

In addition, we ran the algorithms on real-life images. Two pictures of Beethoven's bust were inputs to the backward and forward semi-Lagrangian schemes (Fig. 6). The backward reconstruction (Fig. 6c) emphasizes the reconstructed lips, right eye, hair and scarf, whereas the forward one (Fig. 6d), the three dimensional reconstructed nose with two distinguishable nostrils, left eye and shirt. Some inaccurate folds in the reconstructions seem to result from inaccurate boundary conditions and inaccurate measurement of camera parameters (focal length), leading to some accumulation of error.

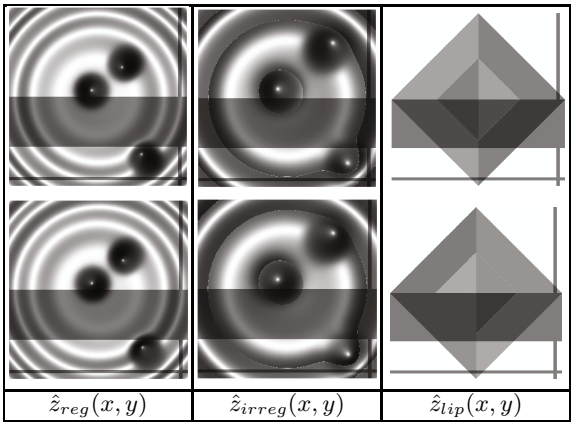

Fig. 3. Perspective images of the respective surfaces of Fig. 2, used as inputs to the algorithms. The light source directions, expressed in spherical coordinates $\omega = (\sin(\varphi)\cos(\theta), \sin(\varphi)\sin(\theta), \cos(\varphi))$, are $\varphi_1 = 0.1 + \pi$, $\theta_1 = 0.0$ for I_1 (in the first row) and $\varphi_2 = 0.1 + \pi$, $\theta_2 = \frac{3\pi}{4}$ for I_2 (in the second row). The albedo on the dark stripe of each image is $\rho = 0.5$; otherwise, $\rho = 1$.

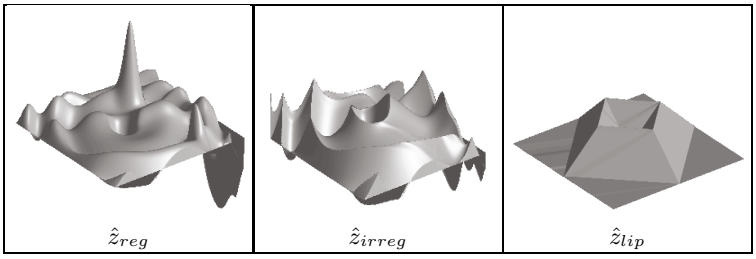

Fig. 4. Reconstruction by the orthographic backward semi-Lagrangian scheme presented in [16,17] using the input images of Fig. 3 (for original surfaces see Fig. 2). The reconstruction is inaccurate. We present the backward semi-Lagrangian reconstruction as it produced the best result among orthographic methods.

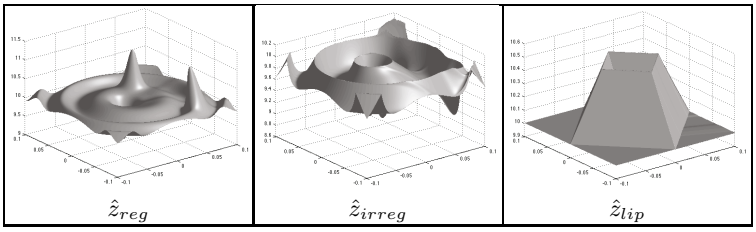

Fig. 5. Reconstruction by the proposed perspective backward semi-Lagrangian scheme, using the input images of Fig. 3. The surfaces are flipped compared to the original ones (Fig. 2) because of the perspective projection. The original surfaces were faithfully recovered.

Table 1. Convergence and accuracy of the forward numerical schemes for each surface of Fig. 2. For each surface we examined images of size $\Delta \times \Delta$ pixels, and computed three error measures: the L^∞ norm in the perspective coordinate system, RMSE in the perspective system, and RMSE in real-world coordinate system. The L^∞ norm shows convergence is linear (i.e., order 1). The RMSE measures quantify the accurate reconstruction with respect to the original surface.

		semi-lag Forward			up-wind Forward		
	Δ	L^∞	MSE-persp	MSE-real	L^∞	MSE-persp	MSE-real
$\hat{z}_{reg}$	100	7.582×10^{-1}	0.079965	0.08006	6.780×10^{-1}	0.073121	0.073157
	200	3.543×10^{-1}	0.048369	0.04849	3.245×10^{-1}	0.046625	0.046775
	400	1.733×10^{-1}	0.027498	0.027577	1.631×10^{-1}	0.02839	0.028495
	800	8.567×10^{-2}	0.014932	0.014977	8.121×10^{-2}	0.016325	0.016389
$\hat{z}_{irreg}$	100	6.726×10^{-1}	0.11174	0.10957	4.693×10^{-1}	0.11507	0.11299
	200	4.977×10^{-1}	0.067081	0.068095	3.925×10^{-1}	0.078578	0.080503
	400	3.381×10^{-1}	0.037985	0.039874	2.664×10^{-1}	0.051528	0.054701
	800	2.174×10^{-1}	0.020888	0.02254	1.590×10^{-1}	0.035682	0.038287
$\hat{z}_{lip}$	100	1.136×10^{-1}	0.0037728	0.003863	1.165×10^{-1}	0.0036506	0.0037189
	200	5.723×10^{-2}	0.001627	0.0016577	6.459×10^{-2}	0.0016576	0.001682
	400	2.681×10^{-2}	0.0010702	0.0011037	3.069×10^{-2}	0.0010969	0.0011326
	800	1.280×10^{-2}	0.00048774	0.00049765	1.531×10^{-2}	0.00050909	0.00051989

Table 2. Convergence and accuracy of the backward numerical schemes for each surface of Fig. 2. The table is organized similarly to Table 1. The rate of convergence of the backward algorithm is the same as of the forward schemes (order 1). Accurate reconstruction is also achieved by the backward schemes.

		semi-lag Backward			up-wind Backward		
	Δ	L^∞	MSE-persp	MSE-real	L^∞	MSE-persp	MSE-real
$\hat{z}_{reg}$	100	7.582×10^{-1}	0.024478	0.025474	2.399×10^{-1}	0.0094924	0.011658
	200	1.789×10^{-1}	0.013978	0.014514	9.918×10^{-2}	0.0061304	0.007485
	400	8.494×10^{-2}	0.007591	0.0078847	4.662×10^{-2}	0.003698	0.0045026
	800	4.113×10^{-2}	0.003997	0.0041618	2.279×10^{-2}	0.0021912	0.0026803
$\hat{z}_{irreg}$	100	2.929×10^{-1}	0.040556	0.042861	1.673×10^{-1}	0.029009	0.028976
	200	2.952×10^{-1}	0.020974	0.023794	1.025×10^{-1}	0.019232	0.019162
	400	2.014×10^{-1}	0.012261	0.014336	8.878×10^{-2}	0.015983	0.016061
	800	1.697×10^{-1}	0.0072217	0.0086446	8.930×10^{-2}	0.014743	0.015029
$\hat{z}_{lip}$	100	1.136×10^{-1}	0.014512	0.015132	1.655×10^{-2}	0.014545	0.015172
	200	2.533×10^{-2}	0.0069519	0.0072408	4.790×10^{-3}	0.0069325	0.0072236
	400	2.681×10^{-2}	0.0035051	0.0036479	5.390×10^{-3}	0.003477	0.0036198
	800	4.600×10^{-3}	0.0017174	0.0017869	1.720×10^{-3}	0.0017049	0.0017746

Table 3. Convergence and accuracy of the orthographic semi-Lagrangian scheme [16] for each surface of Fig. 2. For each surface we examined images of size $\Delta \times \Delta$ pixels, and computed three error measures: the L^∞ norm in the perspective coordinate system, RMSE in the perspective system, and RMSE in real-world coordinate system. The L^∞ norm shows the scheme does not converge. The RMSE is at least an order of magnitude larger than with the proposed method (cf. Tables. 1 and 2).

		Forward			Backward		
	Δ	L^∞	MSE-persp	MSE-real	L^∞	MSE-persp	MSE-real
$\hat{z}_{reg}$	100	9.718×10^{-1}	0.13611	0.13944	1.014	0.13751	0.14127
	200	9.712×10^{-1}	0.13817	0.14188	1.032	0.14018	0.1441
	400	9.674×10^{-1}	0.13976	0.14366	1.037	0.14209	0.14618
	800	9.660×10^{-1}	0.14085	0.14485	1.038	0.14334	0.14757
$\hat{z}_{irreg}$	100	9.759×10^{-1}	0.192	0.18963	9.585×10^{-1}	0.19158	0.19105
	200	9.772×10^{-1}	0.19725	0.19511	9.386×10^{-1}	0.19695	0.19702
	400	9.761×10^{-1}	0.20061	0.19862	9.230×10^{-1}	0.20038	0.20093
	800	9.757×10^{-1}	0.20283	0.20091	9.181×10^{-1}	0.20267	0.20352
$\hat{z}_{lip}$	100	5.641×10^{-1}	0.2042	0.2091	5.658×10^{-1}	0.20459	0.20948
	200	5.703×10^{-2}	0.20555	0.21053	5.713×10^{-2}	0.20544	0.2104
	400	5.758×10^{-2}	0.20626	0.21125	5.753×10^{-2}	0.20594	0.21091
	800	5.787×10^{-2}	0.20661	0.21162	5.792×10^{-2}	0.20621	0.21119

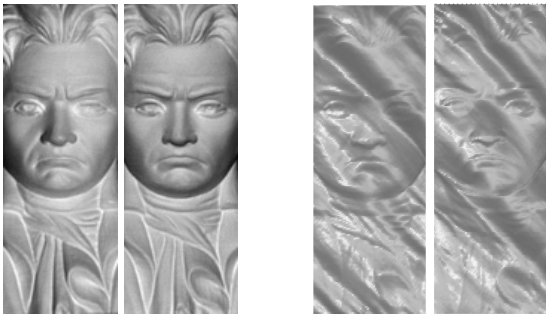

(a) (b) (c) (d)

Fig. 6. Reconstruction of real-life images of the Beethoven bust (a, b) by the backward (c) and forward (d) semi-Lagrangian schemes (frontal view of the rendered reconstructed surfaces). Illumination directions: (a) $\varphi = 15.1^{\circ}, \theta = 72.5^{\circ}$, (b) $\varphi = 11.5^{\circ}, \theta = 184.9^{\circ}$. Focal length: $f = 100$.

7 Conclusions

This study utilized numerical schemes commonly used in the Shape-from-Shading literature also for the 2-image photometric stereo problem under the perspective projection assumption. We proved the uniqueness of the solution in the class of Lipschitz continuous surfaces given Dirichlet boundary conditions. We then extended the two numerical methods of Mecca and Falcone [16], the up-wind finite difference scheme and the Semi-Lagrangian scheme, for the solution of the 2-image *perspective* photometric stereo problem. We compared the suggested method with that of Mecca and Falcone [16] on synthetic examples, and showed that the suggested perspective semi-Lagrangian and up-wind schemes outperformed their method. As the method of Mecca and Falcone [16,17] can also reconstruct the albedo in a manner similar to the suggested perspective one, the inaccurate orthographic reconstruction is not due to the non-constant albedo, but rather a result of the more realistic set of assumptions of a perspective projection in the proposed algorithms. We also demonstrated the ability of the our method to reconstruct real-life images. Our results thus demonstrate that numerical methods of the type common in the Shape-from-Shading literature may provide additional information for solving a perspective photometric stereo problem, as presented here for a 2-image input problem.

References

1. Horn, B.K.P.: Image intensity understanding. Artificial Intelligence 8, 201–231 (1977)
2. Woodham, R.J.: Photometric stereo: A reflectance map technique for determining surface orientation from a single view. In: Proc. SPIE Annual Technical Symposium on Image Understanding Systems and Industrial Applications, San Diego, CA, pp. 136–143 (1978)

3. Woodham, R.J.: Photometric method for determining surface orientation from multiple images. Optical Engineering 19, 139–144 (1980)
4. Tankus, A., Sochen, N., Yeshurun, Y.: Shape-from-Shading under perspective projection. International Journal of Computer Vision 63, 21–43 (2005)
5. Tankus, A., Sochen, N., Yeshurun, Y.: A new perspective [on] Shape-from-Shading. In: Proceedings of the 9th IEEE International Conference on Computer Vision, Nice, France, vol. II, pp. 862–869 (2003)
6. Tankus, A., Sochen, N., Yeshurun, Y.: Perspective Shape-from-Shading by Fast Marching. In: Proceedings of the IEEE Computer Society Conference on Computer Vision and Pattern Recognition, Washington, DC, vol. I, pp. 43–49 (2004)
7. Tankus, A., Sochen, N., Yeshurun, Y.: Reconstruction of medical images by perspective Shape-from-Shading. In: Proceedings of the International Conference on Pattern Recognition, Cambridge, UK, vol. 3, pp. 778–781 (2004)
8. Prados, E., Faugeras, O.D.: "Perspective shape from shading" and viscosity solutions. In: ICCV, pp. 826–831. IEEE Computer Society (2003)
9. Prados, E., Soatto, S.: Fast Marching Method for Generic Shape from Shading. In: Paragios, N., Faugeras, O., Chan, T., Schnörr, C. (eds.) VLSM 2005. LNCS, vol. 3752, pp. 320–331. Springer, Heidelberg (2005)
10. Courteille, F., Crouzil, A., Durou, J.D., Gurdjos, P.: Towards shape from shading under realistic photographic conditions. In: ICPR (2), pp. 277–280 (2004)
11. Argyriou, V., Petrou, M., Hawkes, P.W.: Chapter 1 photometric stereo: An overview. In: Advances in Imaging and Electron Physics, vol. 156, pp. 1–54. Elsevier (2009)
12. Okatani, T., Deguchi, K.: On uniqueness of solutions of the three-light-source photometric stereo: Conditions on illumination configuration and surface reflectance. CVIU 81, 211–226 (2001)
13. Shashua, A.: On photometric issues in 3D visual recognition from a single 2D image. International Journal of Computer Vision 21, 99–122 (1997)
14. Basri, R., Jacobs, D., Kemelmacher, I.: Photometric stereo with general, unknown lighting. International Journal of Computer Vision 72, 239–257 (2007)
15. Onn, R., Bruckstein, A.M.: Integrability Disambiguates Surface Recovery in Two-Image Photometric Stereo. International Journal of Computer Vision 5, 105–113 (1990)
16. Mecca, R., Falcone, M.: Uniqueness and approximation of a photometric shape-from-shading model. SIAM Journal on Imaging Sciences (2012) (submitted)
17. Mecca, R.: Uniqueness for shape from shading via photometric stereo technique. In: Macq, B., Schelkens, P. (eds.) IEEE ICIP, pp. 2933–2936 (2011)
18. Kozera, R.: Existence and uniqueness in photometric stereo. Applied Mathematics and Computation 44, 103 (1991)
19. Tankus, A., Kiryati, N.: Photometric stereo under perspective projection. In: Proceedings of the Tenth International Conference on Computer Vision, Beijing, China (2005)
20. Yoon, K.J., Prados, E., Sturm, P.: Generic Scene Recovery using Multiple Images. In: Tai, X.-C., Mørken, K., Lysaker, M., Lie, K.-A. (eds.) SSVM 2009. LNCS, vol. 5567, pp. 745–757. Springer, Heidelberg (2009)
21. Tankus, A., Sochen, N.A., Yeshurun, Y.: Shape-from-shading under perspective projection. International Journal of Computer Vision 63(1), 21–43 (2005)
22. Quarteroni, A., Valli, A.: Numerical Approximation of Partial Differential Equations. Springer (1994)
23. Strickwerda, J.: Finite Difference Schemes and PDE. Wadsworth Brooks/Cole (1989)